

**Far-infrared measurements of oxygen-doped polycrystalline $\text{La}_2\text{CuO}_{4.0315}$
superconductor under slow-cooled and fast-cooled conditions**

Y. H. Kim¹⁺, H. H. Hsieh^{2*}, Z. Wu² and P. H. Hor²⁺⁺

¹Department of Physics, University of Cincinnati, Cincinnati, Ohio 45221-0011, U.S.A.

²Department of Physics and the Texas Center for Superconductivity
University of Houston, Houston, Texas 77204-5005, U.S.A.

We have studied the far-infrared (far-IR) charge dynamics of an equilibrated pure oxygen doped $\text{La}_2\text{CuO}_{4.0315}$ under slow-cooled and fast-cooled conditions. The superconducting transition temperature (T_c) for the slow-cooled and that for the fast-cooled processes were respectively found to be close to the two intrinsic T_c 's: One at 30 K and the other at 15 K. Direct comparison with our previous results and other far-IR and Raman studies on single crystalline $\text{La}_{2-x}\text{Sr}_x\text{CuO}_4$, we conclude that the topology of the pristine electronic phases that are responsible for the two intrinsic T_c 's is holes arranged into two-dimensional (2D) square lattices.

PACS number: 74.25.Gz, 74.72.-h, 78.30.-j

*Present address: Department of Electrical Engineering, Chung Cheng Institute of Technology, National Defense University, Taoyuan, 335 Taiwan, R.O.C.

+ email address: kimy@ucmail.uc.edu

++ email address: phor@uh.edu

High T_c superconductivity (HTS) in doped cuprates still remains enigmatic to the majority in the high T_c research community. This is mainly due to the lack of a unified picture of the underlying electronic states responsible for the nano-scale electronic inhomogeneity¹ in the doping-induced charge carrier (hole) distribution in the CuO_2 planes. This hallmark of cuprate physics is now widely, though not universally², accepted as one of the natural consequences of the electronic phase separation. One possible candidate that we proposed³ for the underlying pristine electronic phase (PEP) responsible for the nano-scale phase separation was the 2D electronic square lattices on which the itinerant holes “ride”. Since the planar hole density (P_{pl})⁴ is one of the most important controlling parameters of the HTS, it is plausible to assess that the generic electronic phase diagram, in which a superconducting dome exists in a narrow range between $P_{\text{pl}} \sim 0.06$ (or 0.11) and 0.25, arises from the presence of the PEP’s and their interaction with the itinerant holes⁵.

Hence, any theoretical model built on the premise where *all* the holes are itinerant in the CuO_2 planes cannot readily answer a question like “How could HTS emerge from such highly inhomogeneous electronic texture?” Consequently, theoretical interpretations to date have offered only a partial explanation for the data obtained by a particular experimental probe but fail to account for the rest observed through different probes, making numerous experimental data seem anomalous. Therefore, one may logically conclude that the missing key step in building the correct microscopic model is the pinning down of the origin of this ubiquitous electronic inhomogeneity and its role in the HTS.

At this point we need to bring out the two subtle but quite important experimental facts that have been overlooked so far. The first is the presence of the distinct onset P_{pl} ’s for the HTS at $P_{\text{pl}} \sim 0.06$ (or 0.11) for the entire family of cuprate superconductors^{4,5}. The second is the

finding that only a small fraction of the holes are participating in the HTS. It was found that ~ 20% of the total holes are itinerant at optimal doping^{6,7} and only ~ 1% in the underdoped $\text{La}_{2-x}\text{Sr}_x\text{CuO}_{4+\delta}$ ^{3,8,9}. What is more fascinating is that the remaining 80% – 99% of the holes in the CuO_2 planes comprise the PEP's in the form of electronic lattices (EL's) as evidenced by the presence of the charge collective modes at finite frequencies and the accompanying single particle excitation gap at $\sim 400 \text{ cm}^{-1}$, which is a direct proof that the EL's are self-organized and pinned^{3,8,9}.

In this work, we chose to study a polycrystalline $\text{La}_2\text{CuO}_{4+\delta}$ at $\delta = 0.0315$ which translates into $P_{\text{pl}} = 0.063$, right above the onset P_{pl} for the HTS. Previous systematic studies of the preparations and the doping efficiency of pure oxygen-doped $\text{La}_2\text{CuO}_{4+\delta}$ and oxygen and strontium co-doped $\text{La}_{2-x}\text{Sr}_x\text{CuO}_{4+\delta}$ (CD-La214) polycrystalline samples found that delicate electrochemical oxidation performed at an elevated temperature (T) and long time post-annealing are required in order to achieve the thermodynamic equilibrium state^{10,11}. These equilibrium samples have only two intrinsic superconducting transitions with $T_c = 15 \text{ K}$ and $T_c = 30 \text{ K}$ ¹⁰, which is independently confirmed later¹². The two intrinsic $T_c = 15 \text{ K}$ and $T_c = 30 \text{ K}$ phases are not owing to the phase separation of the dopant oxygen atoms between the CuO_2 planes – these are the energetically favored electronic states as demonstrated in the studies of the electronic phase diagram of pure oxygen-doped $\text{La}_2\text{CuO}_{4+\delta}$ and CD-La214 polycrystalline samples under high pressure¹³. Although it was in a different context, the earlier studies of the hole cluster diffusion and oxygen diffusion in $\text{La}_2\text{CuO}_{4+\delta}$ as well as the electronic phase separation of the holes also reached the same conclusion.¹⁴

It was also found that depending on the cooling rate, one of the two superconducting phases could be selectively stabilized in $\text{La}_2\text{CuO}_{4+\delta}$ system. For instance, when the sample is

cooled slowly down to 200 K above which the dopant oxygen atoms are highly mobile, the energetically most favored $T_c = 30$ K superconducting state results. However, the T_c of the $\text{La}_2\text{CuO}_{4+\delta}$ with $P_{\text{pl}} \leq 1/16$, which always exhibits the $T_c = 30$ K superconductivity on slow cooling, can be brought to 15 K via quenching. Therefore, here we have a unique opportunity to test whether or not the notion of the mutually exclusive competing order is indeed operating behind the scene because, if they are mutually exclusive, the quenching process should induce EL's. Furthermore, our experiment eliminates the extrinsic disorder effects that may arise from two different samples at two different doping levels, guaranteeing that the observed changes are intrinsic.

For quenching, the sample mounted on the cold finger of a continuous liquid helium flow cryostat was submerged in liquid N_2 . The quenching from room T down to 77 K took less than 1 minute. Once the T of the cold finger starts to drop below 77 K, the sample assembly was placed in the spectrometer for the reflectivity measurements. The entire procedure was done in a dry N_2 gas atmosphere. The slow cooling of the sample was performed under the normal operating condition of the cryostat by adjusting the temperature step by step at the cooling rate $\Delta T/\Delta t = -1$ K/min down to $T = 160$ K and then rapidly cooled down to $T = 10$ K. All the far-IR measurements were done on warming up of the sample from $T = 10$ K.

The magnetic measurements were carried out in a magnetometer and the dc conductivity was measured by using a standard four-probe technique. Fig. 1a clearly shows superconductivity at $T_c \sim 20$ K upon quenching and at $T_c \sim 30$ K when slow-cooled. It is interesting to note that while both cases reached zero resistance, the resistivity of the quenched sample is “lower” than that of the slow-cooled one (see Figure 1b), which is a clear indication that the quenching process creates a larger fraction of “metallic” region corresponding to a $T_c \sim 20$ K. The quenched

and slow-cooled resistivity and magnetic susceptibility data were measured by following closely to the quenched and slow-cooled processes of the far-IR measurements.

The far-IR reflectivities of the quenched and of the slow-cooled sample at various T 's are displayed in Fig. 2. Overall reflectivity increases systematically with decreasing T . The reflectivity minimum at $\omega \sim 15 \text{ cm}^{-1}$ and the peak at $\omega \sim 23 \text{ cm}^{-1}$ are commonly present for both quenched and slow-cooled sample. Also a small peak develops at $\omega \sim 100 \text{ cm}^{-1}$ in both cases with decreasing T . The intense mode at $\omega \sim 220 \text{ cm}^{-1}$ (denoted as C in Figure 3) is the well-known c-axis breathing mode of the apical oxygen.

$\sigma_1(\omega)$ and $\varepsilon_1(\omega)$ calculated from the reflectivity data using a Kramers-Kronig transformation³ are displayed in Fig. 3. The origin of the reflectivity minimum in both the slow-cooled and the quenched sample at $\omega \sim 15 \text{ cm}^{-1}$ becomes clear; this is the characteristic of the plasma behavior of the free carriers in the system. The small value of ω_p suggests that the ratio of the free hole density to the hole mass is extremely small. In the $\sigma_1(\omega)$ plot for the quenched sample, the two peaks indicated as G_1 and P develop as T is lowered below 300 K and there also develop a broad structure between the G_1 and P modes.

Upon slow cooling, in addition to the G_1 and P modes observed in the quenched sample, two new modes (G_2 at $\omega \sim 43 \text{ cm}^{-1}$ and G_3 at $\omega \sim 62 \text{ cm}^{-1}$) emerge out of the broad structure and the $T_c = 30 \text{ K}$ superconductivity results. Thus, one may conclude that the development of the G_2 (and G_3) mode must be related to the $T_c = 30 \text{ K}$ superconductivity. In fact, the previous far-IR studies of the CD-La214³ found that the development of the G_2 peak is essential for having the $T_c = 30 \text{ K}$ superconductivity and it was suggested that this G_2 mode is the charge collective mode of the c(2x2) EL.^{3,8} The single particle excitation gap $2\Delta \sim 400 \text{ cm}^{-1}$ (50 meV) for both quenched and slow-cooled sample was estimated from the zero-crossing in $\varepsilon_1(\omega)$. However, this zero-

crossing frequency must be higher than the actual zero-crossing of the gap because of the extra negative contributions to $\epsilon_1(\omega)$ by the phonons. Notice that there is a discrepancy in the reflectivity obtained at 300 K under the quenched and the slow-cooled conditions (see Fig. 2). This is because it takes a substantial amount of time to “anneal away” the localized carriers in the EL sites even at room T once the EL’s are formed.

The development of the P mode upon doping along with the G modes deserves special attention because, although the P mode appears as a weak mode in the polycrystalline sample, this mode is dominating the in-plane $\sigma_1(\omega)$ of single crystalline $\text{La}_{2-x}\text{Sr}_x\text{CuO}_4$ ^{9,15}. As shown in Fig. 4, direct comparison reveals that the P mode seen in the polycrystalline $\text{La}_2\text{CuO}_{4.0315}$ is a superposition of the two modes, one (Z mode) at $\sim 100 \text{ cm}^{-1}$ which develops at low T and the other (X_1 mode) at $\sim 110 \text{ cm}^{-1}$ at low T which is red-shifted from $\sim 140 \text{ cm}^{-1}$ at room T . This Z mode must be related to the charge dynamics along the c-axis because it is absent in the in-plane $\sigma_1(\omega)$ of the single crystal sample. There also commonly presents a weaker but sharper mode at $\sim 360 \text{ cm}^{-1}$ indicated as X_2 .

These Z, X_1 and X_2 modes also appear in the Raman studies^{16,17}. Lack of oxygen isotope effect on the Z mode and the X_1 mode in the Raman spectra¹⁶ suggests that these are related to the motion of the La/Sr atom connected to the apical oxygen atom of each octahedron. The Z mode is highly polarized along the c-axis and the X_1 and X_2 modes are highly polarized along the CuO_2 plane. However the X_2 mode follows the mass harmonic law upon oxygen isotope substitution meaning that it is related to the apical oxygen vibration mode parallel to the CuO_2 plane¹⁶. It was also found that these Z, X_1 and X_2 modes developed only for the P_{pl} range between 0.03 and 0.27, consistent with the far-IR observation. The Raman intensities of these modes

mainly depended on the amount of doping and the local lattice distortions induced by doping, suggesting that the inversion symmetry breaking takes place due to the EL formation¹⁷.

The asymmetric line shape of the X_1 mode is due to the Fano-type coupling¹⁸, clearly indicating the strong phonon–EL interaction. The linewidth of X_1 mode in the polycrystalline sample ($\sim 8 \text{ cm}^{-1}$) is much narrower than that of the single crystalline sample ($\sim 40 \text{ cm}^{-1}$) at low T , suggesting that the degree of electronic disorder in the single crystalline sample is much more severe as pointed out in Ref.[9]. We point out that the ratio of the oscillator strength of the X_1 mode of the polycrystalline sample to that of the single crystalline sample is ~ 0.02 . In other words, the spectral contribution of the CuO_2 plane to the reflectivity of the polycrystalline sample is only $\sim 2\%$. Since the X_1 mode is highly in-plane polarized, it is expected to be more dominating the in-plane $\sigma_1(\omega)$ of the single crystalline sample as the angle of incidence approaches the normal incidence^{9,15}.

One-dimensional (1D) charge stripe order as the topology of the EL in the $\text{La}_{2-x}\text{Sr}_x\text{CuO}_{4+\delta}$ system was proposed based on the neutron study of $\text{La}_{1.6-x}\text{Nd}_{0.4}\text{Sr}_x\text{CuO}_4$ at $P_{\text{pl}} \sim 1/8$.¹⁹ Since superconductivity in $\text{La}_{2-x}\text{Sr}_x\text{CuO}_{4+\delta}$ is suppressed at $P_{\text{pl}} \sim 1/8$, this was attributed to the charge stripe formation at $P_{\text{pl}} \sim 1/8$. Then, according to this scenario, the static charge stripes must melt or become dynamic to bring about the HTS, which implies the diminishing of the oscillator strength of EL modes away from $P_{\text{pl}} \sim 1/8$. This is not what has been seen in this work.

The previous electrochemical doping studies and the far-IR studies of $\text{La}_{2-x}\text{Sr}_x\text{CuO}_{4+\delta}$ led us to conclude that the PEP formed at $P_{\text{pl}} \sim 0.06$ corresponds to a 2D EL of $p(4 \times 4)$ symmetry where $P_{\text{pl}} = 1/16 = 0.0625$ which supports the $T_c = 15 \text{ K}$ superconductivity. Upon further increasing the P_{pl} the 2D EL of $c(2 \times 2)$ symmetry ($P_{\text{pl}} = 1/8 = 0.125$) emerges and the $T_c = 30 \text{ K}$ superconductivity results. Indeed, recent experimental evidences seem to agree with this

observation that the intrinsic T_c 's of the HTS is tied to specific PEP's of $P_{pl} = 1/16 (= 1/4^2)$, $1/8 (= 2/4^2)$, $1/9 (= 1/3^2)$, $3/16 (= 3/4^2)$, and $1/4 (= 4/4^2)$, which naturally leads to the 2D EL's²⁰. However, the far-IR evidence for the 2D nature of the EL was deduced from the line shape of the single particle excitation peak that lacks the characteristics of the 1D EL³.

In principle it is possible to test the dimensionality of the EL's by measuring the far-IR in-plane anisotropy. This has not been feasible for our polycrystalline samples and even for single crystalline samples because of the twinning problem. Fortunately, Padilla *et al*²¹ reported detailed far-IR studies of the de-twinned $\text{La}_{2-x}\text{Sr}_x\text{CuO}_4$ single crystals as a function of doping for two polarizations, one along the a -axis and the other along the b -axis of the CuO_2 plane. They observed the broad peak at $\sim 110 \text{ cm}^{-1}$ in both directions²². This broad peak at $\sim 110 \text{ cm}^{-1}$ is the charge-induced X_1 mode described in this paper and its strength is already dominating even at $\sim 4\%$ doping. Therefore, there is no intrinsic anisotropy in the in-plane far-IR spectra and the EL is indeed 2D in nature.

In light of the two intrinsic superconducting phases ($T_c = 15 \text{ K}$ and $T_c = 30 \text{ K}$) observed in the $\text{La}_2\text{CuO}_{4+\delta}$ in thermal equilibrium, one may conclude that the $T_c = 20 \text{ K}$ superconducting state observed in the quenched sample is an admixture of the $T_c = 15 \text{ K}$ phase and of the $T_c = 30 \text{ K}$ phase. Hence the G_2 mode (and G_3 mode) is also present in the quenched sample but they appear as a broad bump. Upon slow-cooling, the G_2 mode dominates and the $T_c = 30 \text{ K}$ state is obtained. However we believe that the long-range order of the $P_{pl} = 3/16$ EL of the G_3 mode, which should correspond to the $T_c = 45 \text{ K}$ phase, was not fully developed to support the $T_c = 45 \text{ K}$ superconductivity²³ and must have been present in the form of small disconnected patches in the CuO_2 planes.

In conclusion, we have verified the 2D nature of the EL through detailed analysis of the charge-induced infrared modes. Our observation is contrary not only to the notion of the mutually exclusive competing order but also to the 1D static/dynamic charge stripe order as the topology of the EL. In this work, we have identified for the first time the physical origin of the mysterious intense structure at $\sim 110 \text{ cm}^{-1}$ that has been misunderstood as a charge stripe related structure.²⁴ We have demonstrated that the presence of 2D EL is essential for the appearance of the HTS. The severe electronic disorder in the single crystalline sample suggests mixing of the disordered EL's of various symmetries⁹. We anticipate, therefore, inhomogeneous local gaps in the STM experiments since the so-called pseudo gap is the single particle excitation gap of an EL²⁵. The STM observation of the co-existence of 100% coverage of the nano-scale inhomogeneous local gaps with HTS²⁶ and the non-competing nature of the pseudo gap against HTS²⁷ is consistent with our composite picture of a small amount of free carriers moving on the mixed 2D EL's that form the condensate below T_c ²⁸.

We thank Z. G. Li for preparing the equilibrium electrochemically charged $\text{La}_2\text{CuO}_{4.0315}$ sample for us. Z. Wu, Z. G. Li, H. H. Hsieh, and P. H. Hor are supported by the State of Texas through the Texas Center for Superconductivity at the University of Houston.

References:

1. S.H. Pan, J.P. O'Neal, R.L. Badzey, C. Chamen, H. Ding, J.R. Engelbrecht, Z. Wang, H. Esaki, S. Uchida, A.K. Gupta, L.-W. Ng, E.W. Hudson, L.M. Lang, J.C. Davis, *Nature* **413**, 282 (2001).
2. J. Bobroff, H. Alloul, S. Ouazi, P. Mendels, A. Mahajan, N. Blanchard, G. Collin, V. Guillen, J.-F Marucco, *Phys. Rev. Lett.* **89**, 1570021 (2002).
3. Y. H. Kim and P. H. Hor, *Mod. Phys. Lett.* **B15**, 497 (2001).
4. T. Honma, P.H. Hor, H.H. Hsieh, and M. Tanimoto, *Phys. Rev. B* **70**, 214517 (2004).
5. According to the P_{pl} calibration scheme proposed by Honma and Hor, the onset is at $P_{pl} \sim 0.11$ for $Y_{1-x}Ca_xBa_2Cu_3O_{7-\delta}$ rather than 0.06. See T. Honma and P.H. Hor, *Phys. Rev. B* **75**, 012508 (2007). Actually cation substituted Y123 and Bi2201 and, possibly Bi2212 are all having a T_c onset at $P_{pl} \sim 0.1$ (see Fig. 8 in Ref. 4).
6. A. V. Pronin, B. P. Gorshunov, A. A. Volkov, H. S. Somal, D. van der Marel, B.J. Finstra, Y. Jaccard, and J.-P. Locquet, *JETP Lett.* **68**, 432 (1998).
7. D. B. Tanner, F. Gao, K. Kamaras, H. L. Liu, M. A. Quijada, D. B. Romero, Y.-D. Yoon, A. Zibold, H. Berger, G. Margaritondo, L. Forro, R. J. Kelly, M. Onellion, G. Cao, J. E. Crow, B.H. O, J. T. Markert, J. P. Rice, D. M. Ginzberg, and Th. Wolf, *Physica C* **341-348**, 2193 (2000).
8. P. H. Hor and Y. H. Kim, *J. Phys.: Condensed Matter* **14**, 10377 (2002).
9. Y. H. Kim, P. H. Hor, X. L. Dong, F. Zhou, Z. X. Zhao, Y. S. Song, and W. X. Ti, *J. Phys.: Condensed Matter* **15**, 8485 (2003).
10. H.H. Feng, Z.G. Li, P.H. Hor, S. Bhavaraju, J.F. DiCarlo, and A.J. Jacobson, *Phys Rev.* **B51**, 16499 (1995).
11. Z.G. Li, H.H. Feng, Z.Y. Yang, A. Hamed, S.T. Ting, and P.H. Hor, *Phys. Rev. Lett.* **77**, 5413 (1996).
12. G. Campi and A. Bianconi, *J. Supercond.* **18**, 637 (2005).
13. B. Lorenz, Z.G. Li, T. Honma, and P.H. Hor, *Phys. Rev.* **B65**, 144522 (2002).
14. R.K. Kremer, V. Hizhnyakov, E. Sigmund, A. Simon, K.A. Muller, *Z. Phys.* **B91**, 169 (1993).
15. B. Pignon, G. Gruener, V. Ta Phuoc, F. Gervais, C. Martin, and L. Ammor, *J. Phys.: Condensed Matter* **20**, 075230 (2008).

16. E. Liarakapis, E. Siranidi, D. Lampakis, K. Conder, and C. Panagopoulos, *J. Phys.: Condensed Matter* **20**, 434233(2008).
17. D. Lampakis, E. Liarakapis, and C. Panagopoulos, arXiv:0902.2678.
18. Y.H. Kim and P.H. Hor, to be published.
19. J.M. Tranquada, B.J. Sternlieb, J.D. Axe, Y. Nakamura, and S. Uchida, *Nature* **375**, 561 (1995).
20. See X.L. Dong, P.H. Hor, F. Zhou and Z.-X. Zhao, *Solid State Communications*, **145**, 173 (2008); T. Honma and P.H. Hor, *Phys. Rev. B* **75**, 012508 (2007).
21. W.J. Padilla, M. Dumm, S. Komiya, Y. Ando, and D.N. Basov, *Phys. Rev. B* **72**, 205101 (2005).
22. We believe that the sharp mode observed at $\sim 100 \text{ cm}^{-1}$ in Ref. 21 at 4% doping shares the same physical origin as the $\sim 100 \text{ cm}^{-1}$ mode also seen at 0% doping. The presence of this mode at 4% doping is due to the doping inhomogeneity. Notice that the sharp peak at $\sim 100 \text{ cm}^{-1}$ appear only along the *a*-axis on top of the 110 cm^{-1} broad peak which is present in both *a*- and *b*-axis directions (see the text). This $\sim 100 \text{ cm}^{-1}$ peak should disappear as the doping increases and the dopant distribution becomes more uniform.
23. Y.H. Kim, Y.S. Song, and P.H. Hor (to be published).
24. M. Dumm, S. Komiya, Y. Ando, and D.N. Basov, *Phys. Rev. Lett.* **91**, 077004 (2003).
25. EL's of higher (lower) order symmetries than $p(4 \times 4)$ symmetry ($2\Delta \sim 400 \text{ cm}^{-1}$) should have larger (smaller) gaps. However because of the coexistence of the EL's, the $\sim 400 \text{ cm}^{-1}$ gap always appears as an onset of the gap in far-IR.
26. K.K. Gomes, A.N. Pasupathy, A. Pushp, S. Ono, Y. Ando, and A. Yazdani, *Nature* **447**, 569 (2007). It is clearly shown in Fig. 5 that bulk superconductivity is realized when the CuO_2 plane is completely covered by the inhomogeneous local gaps.
27. K.K. Gomes, A.N. Pasupathy, A. Pushp, S. Ono, Y. Ando, and A. Yazdani, *Physica C* **460-462**, 212 (2007).
28. Y.H. Kim and P.H. Hor, *Mod. Phys. Lett. B* **20**, 571 (2006).

Figure Captions:

Figure 1. (a) The magnetic susceptibility measured under field-cooled at 5 Gauss and (b) the resistivity of the quenched and slow-cooled $\text{La}_2\text{CuO}_{4+0.00315}$. The data is always collected during warming from 5 K.

Figure 2. Far-IR reflectivity of the quenched and slow-cooled $\text{La}_2\text{CuO}_{4+0.0315}$. From bottom to top: $T = 300\text{ K}, 270\text{ K}, 250\text{ K}, 220\text{ K}, 200\text{ K}, 190\text{ K}, 180\text{ K}, 170\text{ K}, 160\text{ K}, 130\text{ K}, 110\text{ K}, 100\text{ K}, 70\text{ K}, 50\text{ K}, 40\text{ K}, 35\text{ K}, 34\text{ K}, 33\text{ K}, 32\text{ K}, 31\text{ K}, 30\text{ K}, 29\text{ K}, 28\text{ K}, 27\text{ K}, 26\text{ K}, 25\text{ K}, 23\text{ K}, 22\text{ K}, 21\text{ K}, 20\text{ K}, 19\text{ K}, 18\text{ K}, 17\text{ K}, 16\text{ K}, 15\text{ K}, 12\text{ K},$ and 10 K . The black lines are for the superconducting state.

Figure 3. Temperature of $\sigma_1(\omega)$ and $\epsilon_1(\omega)$. Black lines indicate the superconducting state. The T in the lower panels decreases from top to bottom.

Figure 4. Direct comparison of the EL-induced modes of $\text{La}_2\text{CuO}_{4+0.0315}$ with those of the $\text{La}_{1.93}\text{Sr}_{0.07}\text{CuO}_4$ single crystal ($T_c \sim 20\text{ K}$). From bottom to top: $T = 300\text{ K}, 200\text{ K}, 100\text{ K}, 50\text{ K}, 30\text{ K}, 24\text{ K}, 16\text{ K},$ and 8 K for $\text{La}_{1.93}\text{Sr}_{0.07}\text{CuO}_4$; $T = 300\text{ K}, 250\text{ K}, 200\text{ K}, 180\text{ K}, 160\text{ K}, 100\text{ K}, 70\text{ K}, 40\text{ K}, 30\text{ K},$ and 10 K for $\text{La}_2\text{CuO}_{4+0.0315}$. Note the log-scale in frequency.

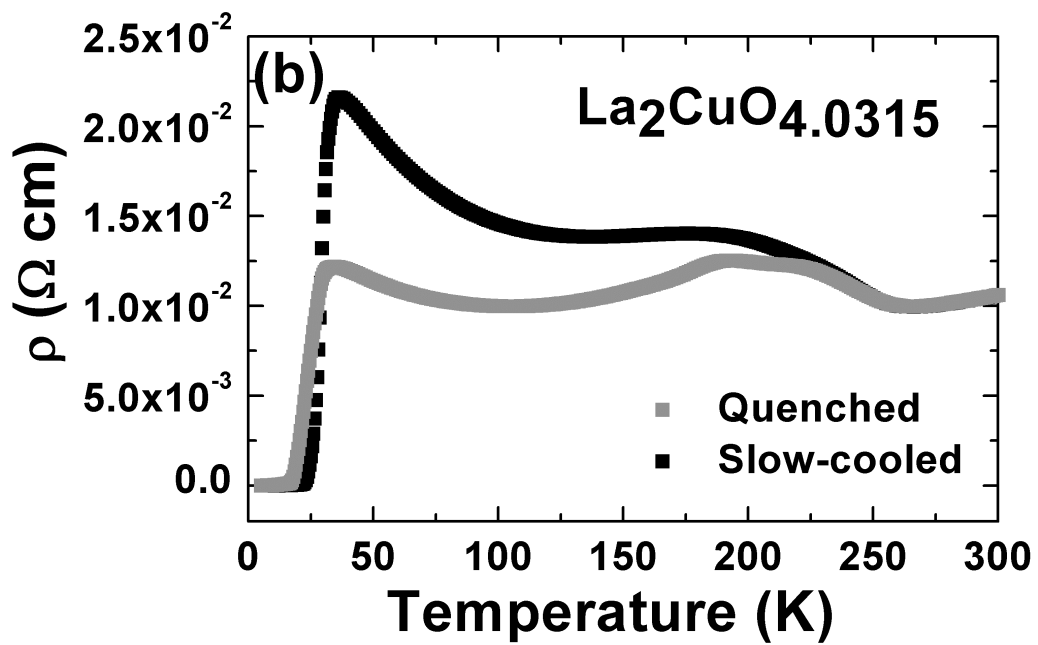
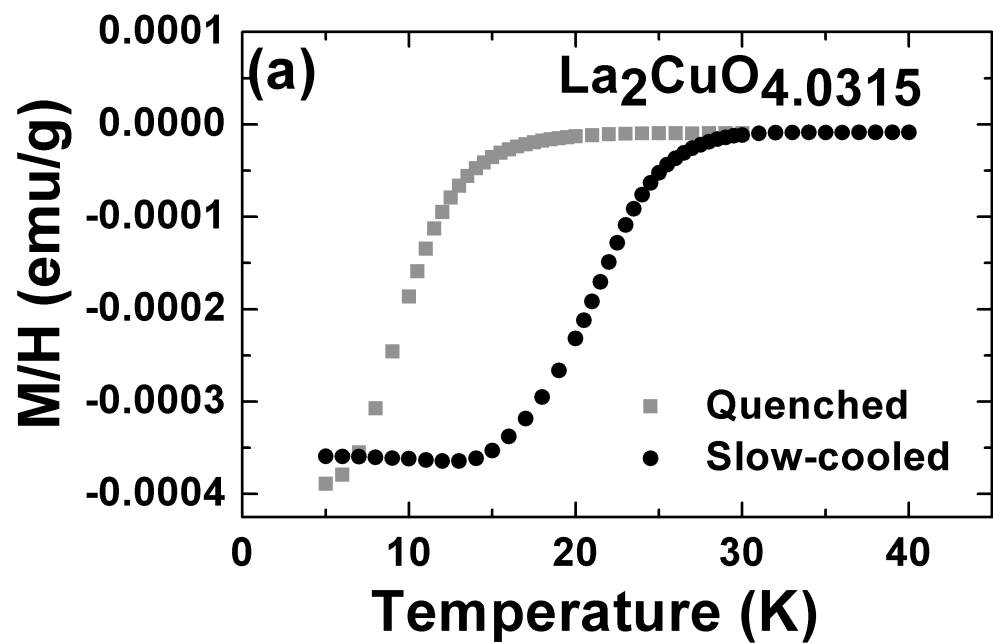


Figure 1

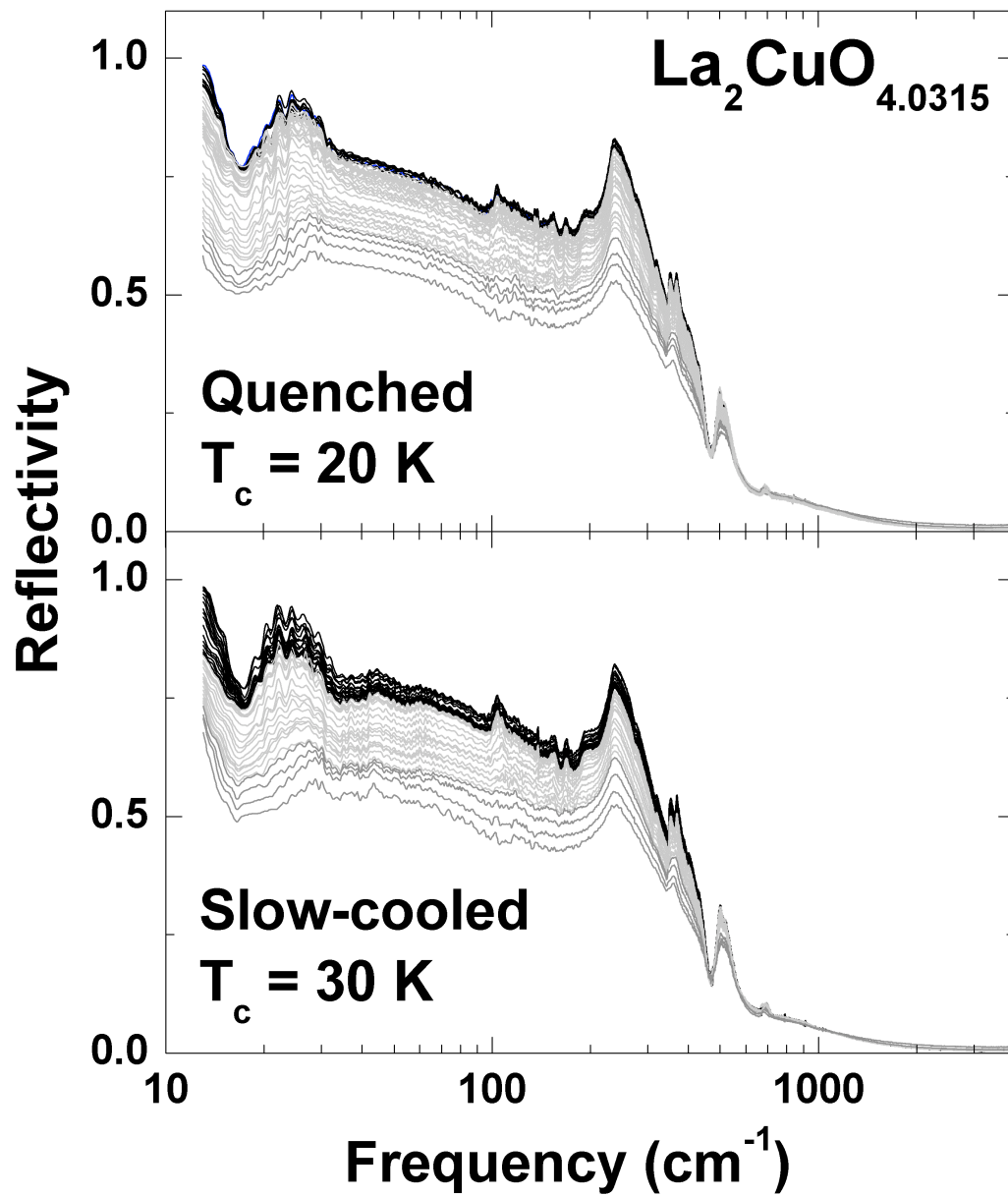


Figure 2

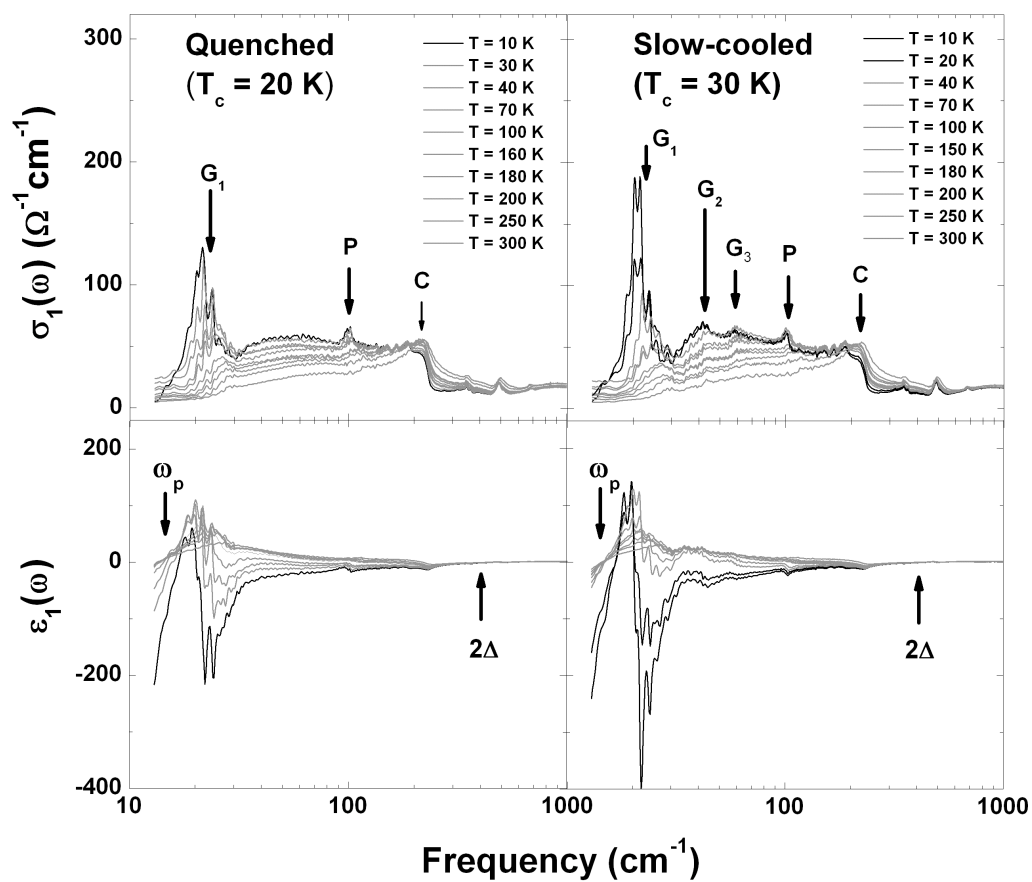


Figure 3

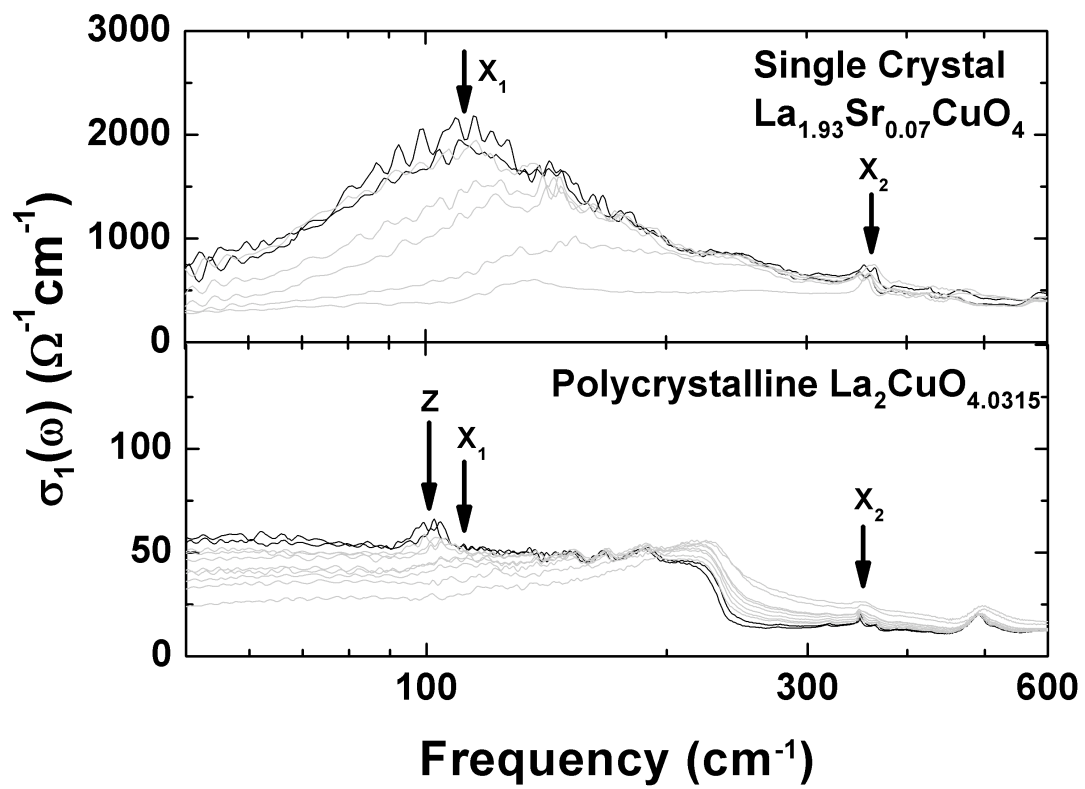


Figure 4